GEOPHYSICS, VOL. 57, NO. 6 (JUNE 1992); P. 781–792, 8 FIGS., 1 TABLE.

Modeling anelastic singular surface waves in the earth

José M. Carcione*

ABSTRACT

The propagation of anelastic surface waves presents substantial differences compared to the elastic case. Therefore, a forward modeling scheme to study surface waves in an anelastic earth is of some relevance to the geophysical problem.

When propagating anelastic waves, accuracy is very important; in particular, numerical dispersion should not be confused with physical velocity dispersion. One modeling algorithm, based on the velocity-stress elastodynamic equations, uses a spectral method with a Chebychev expansion in the vertical direction. This approach allows the calculation of the spatial derivatives with high accuracy, and an effective incorporation of the free surface boundary conditions since the method is not periodic. However, a direct application of the traction-free boundary conditions without regard to the other variables produces numerical instabilities. To solve this problem, a boundary treatment based on characteristics is implemented that results in a wave equation for the surface that automatically includes the boundary conditions.

Two examples of wave propagation in an unconsolidated weathering zone are presented. The first model is homogeneous and the second structure contains a vertical interface separating an anelastic medium from an elastic region. The results indicate that the modeling correctly describes the anelastic properties of Rayleigh waves, even in the presence of a strong contrast in the material parameters.

INTRODUCTION

Anelasticity of earth materials has an important influence on wave propagation, particularly on surface waves, since the weathering zone is generally an unconsolidated medium and therefore shows strong dissipation and velocity dispersion.

Moreover, anelasticity introduces new phenomena not present in the propagation of elastic surface waves (e.g., Carcione, 1992). Considering, for instance, anelastic Rayleigh waves in a homogeneous half-space, there are several differences with the elastic case. In the first place, more than one Rayleigh wave is possible, one of them corresponding to the usual elastic surface wave, and the other, which exists only when the medium is viscoelastic, for certain combinations of the Lamé parameters and for a given range of frequencies. In contrast to elastic materials, for these anelastic surface waves, the particle motion may be either direct or retrograde at the surface. The motion may change sense at many or no levels with depth, and for the second Rayleigh wave, the energy velocity may be greater than the body wave energy velocity. Consequently, a forward modeling scheme to study surface waves in an anelastic earth is of relevance for the geophysical problem. An analysis of anelastic Rayleigh waves by using energy considerations can be found in Carcione (1992) where the energy balance is computed and the quality factors and energy velocity are calculated as a function of frequency, depth, and per unit surface area. A theoretical analysis of wave motion in anelastic media can be done for very simple structures like, for instance, the homogeneous half-space studied in Carcione (1992). However, for more complicated models, wave simulation is needed.

In addition to incorporating all these new effects in wave modeling, accuracy is very important when studying anelastic wave propagation. In particular, velocity dispersion is not to be confused with numerical dispersion. Spatial accuracy is achieved by using pseudospectral methods for computing the spatial derivatives of the anelastic wave equation. This modeling scheme is based on a spatial discretization on a grid in which the spatial derivatives are calculated with a Chebychev method in the vertical direction and a Fourier method for the horizontal direction. This approach allows a

Manuscript received by the Editor June 18, 1991; revised manuscript received December 2, 1991.
*Osservatorio Geofisico Sperimentale, P. O. Box 2011 (Opicina), 34016 Trieste, Italy.

natural incorporation of the free surface boundary condition, since the Chebychev method is not periodic in the vertical direction, and one can handle any source-receiver configuration unlike with the Fourier method. The modeling scheme used in this work was first introduced by Kosloff et al., (1990) to solve wave propagation problems in purely elastic media.

A direct implementation of the free surface boundary conditions may produce instabilities. To avoid this problem, a boundary treatment based on characteristics is applied. The wave equation, recast as a first-order hyperbolic system, is decomposed into wave modes that describe outgoing and incoming waves at the boundaries. The outgoing waves are determined by the solution within the computational volume, while the incoming wave depends on the boundary conditions. The result of this approach is a wave equation at the free surface that automatically includes the boundary conditions.

The first section introduces the 2-D wave equation for linear isotropic-viscoelastic media. Then, the boundary treatment is outlined, and the wave equation at the free surface is obtained. Next follows a description of the numerical modeling algorithm. The first example computes synthetic seismograms and snapshots of Rayleigh wave propagation in a homogeneous anelastic half-space that represents an unconsolidated weathering zone. A second example tests the modeling scheme in a structure containing a vertical interface separating an elastic medium from an anelastic region, and bounded at the top by a free surface.

THE WAVE EQUATION

This description of wave propagation is based on the equation of momentum conservation combined with the constitutive relations for infinitesimal deformations. For 2-D media, the equations of momentum conservation are

$$\dot{v}_x = \frac{1}{\rho}\left(\frac{\partial \sigma_{xx}}{\partial x} + \frac{\partial \sigma_{xz}}{\partial z}\right) + f_x, \tag{1a}$$

$$\dot{v}_z = \frac{1}{\rho}\left(\frac{\partial \sigma_{xz}}{\partial x} + \frac{\partial \sigma_{zz}}{\partial z}\right) + f_z, \tag{1b}$$

where $\mathbf{x} = (x, z)$ are Cartesian coordinates, $\sigma_{xx}(\mathbf{x}, t)$, $\sigma_{xz}(\mathbf{x}, t)$, and $\sigma_{zz}(\mathbf{x}, t)$ are the stress components, $v_x(\mathbf{x}, t)$ and $v_z(\mathbf{x}, t)$ are the particle velocities, $\rho(\mathbf{x})$ denotes the density, and $\mathbf{f}(\mathbf{x}, t) = (f_x, f_z)$ are the body forces per unit volume. In equation (1a and b) and elsewhere, time differentiation is indicated with the dot convention.

The constitutive relations for an isotropic-viscoelastic medium expressed in terms of the particle velocity derivatives are (Carcione et al., 1988; Carcione and Behle, 1989)

$$\dot{\sigma}_{xx} = (\hat{\lambda} + 2\hat{\mu})\frac{\partial v_x}{\partial x} + \hat{\lambda}\frac{\partial v_z}{\partial z} + (\lambda + \mu)\sum_{\ell=1}^{L_1} e_{1\ell} + \mu \sum_{\ell=1}^{L_2} e_{2\ell}, \tag{2a}$$

$$\dot{\sigma}_{zz} = \hat{\lambda}\frac{\partial v_x}{\partial x} + (\hat{\lambda} + 2\hat{\mu})\frac{\partial v_z}{\partial z} + (\lambda + \mu)\sum_{\ell=1}^{L_1} e_{1\ell} - \mu \sum_{\ell=1}^{L_2} e_{2\ell}, \tag{2b}$$

$$\dot{\sigma}_{xz} = \hat{\mu}\left(\frac{\partial v_x}{\partial z} + \frac{\partial v_z}{\partial x}\right) + \mu \sum_{\ell=1}^{L_2} e_{3\ell}, \tag{2c}$$

where

$$\hat{\lambda} = (\lambda + \mu)M_{u1} - \mu M_{u2}, \quad \text{and} \quad \hat{\mu} = \mu M_{u2}, \tag{3a, b}$$

are the high-frequency limit Lamé constants, with λ and μ the elastic Lamé constants, and $M_{u\nu}$, $\nu = 1, 2$ are relaxation functions evaluated at $t = 0$, with $\nu = 1$, the dilatational mode, and $\nu = 2$, the shear mode. For a general standard linear solid rheology, they are given by

$$M_{u\nu} = 1 - \sum_{\ell=1}^{L_\nu}\left(1 - \frac{\tau_{\varepsilon\ell}^{(\nu)}}{\tau_{\sigma\ell}^{(\nu)}}\right), \quad \nu = 1, 2, \tag{4}$$

with $\tau_{\sigma\ell}^{(\nu)}$ and $\tau_{\varepsilon\ell}^{(\nu)}$ material relaxation times. The quantities $e_{1\ell}(\mathbf{x}, t)$ are memory variables related to the L_1 mechanisms which describe the anelastic characteristics of the dilatational wave, and $e_{2\ell}(\mathbf{x}, t)$, $e_{3\ell}(\mathbf{x}, t)$ are memory variables related to the L_2 mechanisms for the quasi-shear wave.

The scheme is completed by the memory variables first-order equations in time:

$$\dot{e}_{1\ell} = \phi_{1\ell}\left(\frac{\partial v_x}{\partial x} + \frac{\partial v_z}{\partial z}\right) - \frac{e_{1\ell}}{\tau_{\sigma\ell}^{(1)}}, \quad \ell = 1, \ldots, L_1, \tag{5a}$$

$$\dot{e}_{2\ell} = \phi_{2\ell}\left(\frac{\partial v_x}{\partial x} - \frac{\partial v_z}{\partial z}\right) - \frac{e_{2\ell}}{\tau_{\sigma\ell}^{(2)}}, \quad \ell = 1, \ldots, L_2, \tag{5b}$$

$$\dot{e}_{3\ell} = \phi_{2\ell}\left(\frac{\partial v_x}{\partial z} + \frac{\partial v_z}{\partial x}\right) - \frac{e_{3\ell}}{\tau_{\sigma\ell}^{(2)}}, \quad \ell = 1, \ldots, L_2, \tag{5c}$$

where

$$\phi_{\nu\ell} = \frac{1}{\tau_{\sigma\ell}^{(\nu)}}\left(1 - \frac{\tau_{\varepsilon\ell}^{(\nu)}}{\tau_{\sigma\ell}^{(\nu)}}\right), \quad \nu = 1, 2. \tag{6}$$

In the elastic limit, $\tau_{\varepsilon\ell}^{(\nu)} \to \tau_{\sigma\ell}^{(\nu)}$; thus, $M_{u\nu} \to 1$ and $\phi_{\nu\ell} \to 0$, and the memory variables vanish. In this case, equations (2a-c) become Hooke's law. As can be seen from the stress-strain equations, the mean stress $(\sigma_{xx} + \sigma_{zz})/2$ depends only on the parameters and memory variables with index $\nu = 1$, which involve dilatational dissipation mechanisms. Similarly, the deviatoric stress components $(\sigma_{xx} - \sigma_{zz})/2$ and σ_{xz} depend on the parameters and memory variables with index $\nu = 2$ involving shear mechanisms.

Equations (1), (2), and (5) together with the boundary conditions completely describe the wave motion of the earth. Let the surface of the earth be flat and normal to the variable z; then, the boundary conditions read

$$\sigma_{zz} = 0, \quad \sigma_{xz} = 0. \tag{7a, b}$$

For a suitable implementation of the boundary conditions, the formulation requires recasting the equation governing wave propagation as

$$-\frac{\partial \mathbf{V}}{\partial t} + \underset{\sim}{\mathbf{A}}\frac{\partial \mathbf{V}}{\partial x} + \underset{\sim}{\mathbf{B}}\frac{\partial \mathbf{V}}{\partial z} + \mathbf{D} = 0, \tag{8}$$

where

$$\mathbf{V} = \begin{bmatrix} v_x \\ v_z \\ \sigma_{xx} \\ \sigma_{zz} \\ \sigma_{xz} \\ \langle \dot{e}_{1\ell} \rangle_{L_1} \\ \langle \dot{e}_{2\ell} \rangle_{L_2} \\ \langle \dot{e}_{3\ell} \rangle_{L_2} \end{bmatrix}, \quad \mathbf{D} = \begin{bmatrix} f_x \\ f_z \\ (\lambda + \mu) \sum_{\ell=1}^{L_1} \dot{e}_{1\ell} + \mu \sum_{\ell=1}^{L_2} \dot{e}_{2\ell} \\ (\lambda + \mu) \sum_{\ell=1}^{L_2} \dot{e}_{1\ell} - \mu \sum_{\ell=1}^{L_2} \dot{e}_{2\ell} \\ \mu \sum_{\ell=1}^{L_2} \dot{e}_{3\ell} \\ \langle -\dot{e}_{1\ell}/\tau_{\sigma\ell}^{(1)} \rangle_{L_1} \\ \langle -\dot{e}_{2\ell}/\tau_{\sigma\ell}^{(2)} \rangle_{L_2} \\ \langle -\dot{e}_{3\ell}/\tau_{\sigma\ell}^{(2)} /_{L_2} \end{bmatrix}, \tag{9a, b}$$

and

$$\underset{\sim}{\mathbf{A}} = \begin{bmatrix} 0 & 0 & \rho^{-1} & 0 & 0 & 0 & \cdots & 0 \\ 0 & 0 & 0 & 0 & \rho^{-1} & 0 & \cdots & 0 \\ \hat{\lambda} + 2\hat{\mu} & 0 & 0 & 0 & 0 & 0 & \cdots & 0 \\ \hat{\lambda} & 0 & 0 & 0 & 0 & 0 & \cdots & 0 \\ 0 & \hat{\mu} & 0 & 0 & 0 & 0 & \cdots & 0 \\ \langle \phi_{1\ell} & 0 & 0 & 0 & 0 & 0 & \cdots & 0 \rangle_{L_1} \\ \langle \phi_{2\ell} & 0 & 0 & 0 & 0 & 0 & \cdots & 0 \rangle_{L_2} \\ \langle 0 & \phi_{2\ell} & 0 & 0 & 0 & 0 & \cdots & 0 \rangle_{L_2} \end{bmatrix},$$

$$\underset{\sim}{\mathbf{B}} = \begin{bmatrix} 0 & 0 & 0 & 0 & \rho^{-1} & 0 & \cdots & 0 \\ 0 & 0 & 0 & \rho^{-1} & 0 & 0 & \cdots & 0 \\ 0 & \hat{\lambda} & 0 & 0 & 0 & 0 & \cdots & 0 \\ 0 & \hat{\lambda} + 2\hat{\mu} & 0 & 0 & 0 & 0 & \cdots & 0 \\ \hat{\mu} & 0 & 0 & 0 & 0 & 0 & \cdots & 0 \\ \langle 0 & \phi_{1\ell} & 0 & 0 & 0 & 0 & \cdots & 0 \rangle_{L_1} \\ \langle 0 & -\phi_{2\ell} & 0 & 0 & 0 & 0 & \cdots & 0 \rangle_{L_2} \\ \langle \phi_{2\ell} & 0 & 0 & 0 & 0 & 0 & \cdots & 0 \rangle_{L_2} \end{bmatrix}. \tag{10a, b}$$

The notation $\langle \ \rangle_{L_\nu}$ denotes a succession of elements from $\ell = 1, \ldots, L_\nu$, $\nu = 1, 2$. The vectors have dimension $m = 5 + L_1 + 2L_2$, and matrices are of size $m \times m$.

Implementation of the boundary conditions along a given direction requires the characteristic equation corresponding to equation (8) in that direction.

THE BOUNDARY TREATMENT

The method used here was recently developed by Thomson (1990). The characteristic equation corresponding to equation (8) is

$$-\underset{\sim}{\mathbf{S}}^{-1}\frac{\partial \mathbf{V}}{\partial t} + \mathcal{H} + \underset{\sim}{\mathbf{S}}^{-1}\mathbf{C}_z = 0, \qquad \mathbf{C}_z = \underset{\sim}{\mathbf{A}}\frac{\partial \mathbf{V}}{\partial x} + \mathbf{D}, \tag{11}$$

or

$$-\frac{\partial \mathbf{V}}{\partial t} + \underset{\sim}{\mathbf{S}}\mathcal{H} + \mathbf{C}_z = 0, \tag{12}$$

where

$$\mathcal{H} \equiv \underset{\sim}{\mathbf{\Lambda}}\underset{\sim}{\mathbf{S}}^{-1}\frac{\partial \mathbf{V}}{\partial z}, \tag{13}$$

and

$$\underset{\sim}{\mathbf{\Lambda}} = \underset{\sim}{\mathbf{S}}^{-1}\underset{\sim}{\mathbf{B}}\underset{\sim}{\mathbf{S}}, \tag{14}$$

with $\underset{\sim}{\mathbf{\Lambda}}$ the diagonal matrix corresponding to $\underset{\sim}{\mathbf{B}}$, and eigenvalues λ_i, $i = 1, \ldots, m$. $\underset{\sim}{\mathbf{S}}$ is formed by the columns of the right eigenvectors of $\underset{\sim}{\mathbf{B}}$. $\mathcal{H}$ includes each decoupled characteristic wave mode in the z-direction. Since the system of equations is hyperbolic, the eigenvalues of $\underset{\sim}{\mathbf{B}}$ are real. Some of the eigenvalues give the characteristic velocities of outgoing and incoming waves at the boundary.

Equation (12) completely defines $\partial \mathbf{V}/\partial t$ at the boundaries in terms of the decoupled outgoing and incoming modes. The boundary conditions are implemented in the following way. Assume that $a \le z \le b$. For points (z, a), compute $\mathcal{H}_i(\lambda_i < 0$ outgoing waves) from equation (13) and $\mathcal{H}_i(\lambda_i > 0$ incoming waves) from the boundary conditions. Similarly, for points (z, b), compute $\mathcal{H}_i(\lambda_i > 0)$ from equation (13) and $\mathcal{H}_i(\lambda_i < 0)$ from the boundary conditions. Then, solve equation (8) for the interior region and equation (12) at the boundaries. For the isotropic-viscoelastic rheology the eigenvalues are:

$$\lambda_1 = \sqrt{\frac{\hat{\lambda} + 2\hat{\mu}}{\rho}} \equiv c_P,$$

$$\lambda_2 = -c_P,$$

$$\lambda_3 = \sqrt{\frac{\hat{\mu}}{\rho}} \equiv c_S,$$

$$\lambda_4 = -c_S,$$

$$\lambda_i = 0, \quad i = 5, \ldots, m, \tag{15}$$

where the subindices P and S denote compressional and shear waves.

The quantities $\mathcal{H}_i$ relevant for the implementation of the boundary conditions are given by

$$\mathcal{H}_1 = \frac{c_P}{\sqrt{2}}\left(\frac{\partial v_z}{\partial z} + \frac{1}{\rho c_P}\frac{\partial \sigma_{zz}}{\partial z}\right), \tag{16a}$$

$$\mathcal{H}_2 = -\frac{c_P}{\sqrt{2}}\left(\frac{\partial v_z}{\partial z} - \frac{1}{\rho c_P}\frac{\partial \sigma_{zz}}{\partial z}\right), \tag{16b}$$

$$\mathcal{H}_3 = \frac{c_S}{\sqrt{2}}\left(\frac{\partial v_x}{\partial z} + \frac{1}{\rho c_S}\frac{\partial \sigma_{xz}}{\partial z}\right), \tag{16c}$$

$$\mathcal{H}_4 = -\frac{c_S}{\sqrt{2}}\left(\frac{\partial v_x}{\partial z} - \frac{1}{\rho c_S}\frac{\partial \sigma_{xz}}{\partial z}\right). \tag{16d}$$

The wave propagation equations in terms of the decoupled outgoing and incoming modes are

$$\dot{v}_x = \frac{1}{\rho}\frac{\partial \sigma_{xx}}{\partial x} + \frac{1}{\sqrt{2}}(\mathcal{H}_3 + \mathcal{H}_4) + f_x, \tag{17a}$$

$$\dot{v}_z = \frac{1}{\rho}\frac{\partial \sigma_{xz}}{\partial x} + \frac{1}{\sqrt{2}}(\mathcal{H}_1 + \mathcal{H}_2) + f_z, \tag{17b}$$

$$\dot{\sigma}_{xx} = (\hat{\lambda} + 2\hat{\mu})\frac{\partial v_x}{\partial x} + \frac{1}{\sqrt{2}}\frac{\lambda}{c_P}(\mathcal{H}_1 - \mathcal{H}_2) + (\lambda + \mu)\sum_{\ell=1}^{L_1} e_{1\ell} + \mu \sum_{\ell=1}^{L_2} e_{2\ell}, \tag{17c}$$

$$\dot{\sigma}_{zz} = \hat{\lambda}\frac{\partial v_x}{\partial x} + \frac{1}{\sqrt{2}}\rho c_P(\mathcal{H}_1 - \mathcal{H}_2) + (\lambda + \mu)\sum_{\ell=1}^{L_1} e_{1\ell} - \mu \sum_{\ell=1}^{L_2} e_{2\ell}, \tag{17d}$$

$$\dot{\sigma}_{xz} = \hat{\mu}\frac{\partial v_z}{\partial x} + \frac{1}{\sqrt{2}}\rho c_S(\mathcal{H}_3 - \mathcal{H}_4) + \mu \sum_{\ell=1}^{L_1} e_{3\ell}, \tag{17e}$$

$$\ddot{e}_{1\ell} = \phi_{1\ell}\left[\frac{\partial v_x}{\partial x} + \frac{1}{\sqrt{2}\,c_P}(\mathcal{H}_1 - \mathcal{H}_2)\right] - \frac{\dot{e}_{1\ell}}{\tau_{\sigma\ell}^{(1)}}, \quad \ell = 1, \ldots, L_1, \tag{17f}$$

$$\ddot{e}_{2\ell} = \phi_{2\ell}\left[\frac{\partial v_x}{\partial x} + \frac{1}{\sqrt{2}\,c_P}(\mathcal{H}_2 - \mathcal{H}_1)\right] - \frac{\dot{e}_{2\ell}}{\tau_{\sigma\ell}^{(2)}}, \quad \ell = 1, \ldots, L_2. \tag{17g}$$

$$\ddot{e}_{3\ell} = \phi_{2\ell}\left[\frac{\partial v_z}{\partial x} + \frac{1}{\sqrt{2}\,c_S}(\mathcal{H}_3 - \mathcal{H}_4)\right] - \frac{\dot{e}_{3\ell}}{\tau_{\sigma\ell}^{(2)}}, \quad \ell = 1, \ldots, L_2. \tag{17h}$$

The equations describing wave propagation are evaluated in form (12) at the z boundaries, where the quantities $\mathcal{H}_i$, representing incoming variables, depend on the boundary conditions. Actually, each $\mathcal{H}_i$ represents a one-way wave motion as indicated in Figure 1. They are the four possible propagating modes traveling perpendicular to the free surface.

FREE SURFACE BOUNDARY CONDITIONS

The method states that for the interior points $a < z < b$, equation (8) must be solved, while for $z = a$ and $z = b$, equations (12) or (17a-h) are used. Those variables $\mathcal{H}_i$, which represent outgoing variables, are calculated from their definitions in equations (16a-d), while those which represent incoming variables are specified from the boundary conditions. At the surface of the earth, the force-free boundary conditions (7) hold. This means that the normal stresses are zero at all times. Thus, the initial conditions at the surface should include $\sigma_{zz} = \sigma_{xz} = 0$, say at $z = b = 0$. The incoming waves correspond to $\lambda_2 = -c_P$ and $\lambda_4 = -c_S$. Then, $\mathcal{H}_2$ and $\mathcal{H}_4$ must be computed from the boundary conditions. From equations (17d) and (17e), σ_{zz} and σ_{xz} will remain zero at the surface if

$$\mathcal{H}_2 = \mathcal{H}_1 + \frac{\sqrt{2}}{\rho c_P} \times \left[\hat{\lambda}\frac{\partial v_x}{\partial x} + (\lambda + \mu)\sum_{\ell=1}^{L_1} \dot{e}_{1\ell} - \mu \sum_{\ell=1}^{L_2} \dot{e}_{2\ell}\right], \tag{18a}$$

$$\mathcal{H}_4 = \mathcal{H}_3 + \frac{\sqrt{2}}{\rho c_S}\left[\hat{\mu}\frac{\partial v_z}{\partial x} + \mu \sum_{\ell=1}^{L_2} \dot{e}_{3\ell}\right]. \tag{18b}$$

Substituting $\mathcal{H}_1$ and $\mathcal{H}_3$ from equations (16a) and (16c) into (18a) and (18b), and the results into equations (17e-h), yield

$$\dot{v}_x = \frac{1}{\rho}\left(\frac{\partial \sigma_{xx}}{\partial x} + \frac{\partial \sigma_{xz}}{\partial z}\right) + \frac{1}{\rho c_S}\left[\hat{\mu}\left(\frac{\partial v_x}{\partial z} + \frac{\partial v_z}{\partial x}\right) + \mu \sum_{\ell=1}^{L_2} \dot{e}_{3\ell}\right] + f_x, \tag{19a}$$

$$\dot{v}_z = \frac{1}{\rho}\left(\frac{\partial \sigma_{xz}}{\partial x} + \frac{\partial \sigma_{zz}}{\partial z}\right) + \frac{1}{\rho c_P}\left[\hat{\lambda}\frac{\partial v_x}{\partial x} + (\hat{\lambda} + 2\hat{\mu})\frac{\partial v_z}{\partial z} + (\lambda + \mu)\sum_{\ell=1}^{L_1} \dot{e}_{1\ell} - \mu \sum_{\ell=1}^{L_2} \dot{e}_{2\ell}\right] + f_z, \tag{19b}$$

$$\dot{\sigma}_{xx} = \frac{4\hat{\mu}(\hat{\lambda} + \hat{\mu})}{\hat{\lambda} + 2\hat{\mu}}\frac{\partial v_x}{\partial x} + \frac{2\hat{\mu}}{\hat{\lambda} + 2\hat{\mu}}(\lambda + \mu)\sum_{\ell=1}^{L_1} \dot{e}_{1\ell} + \frac{2(\hat{\lambda} + \hat{\mu})}{\hat{\lambda} + 2\hat{\mu}}\mu \sum_{\ell=1}^{L_2} \dot{e}_{2\ell}, \tag{19c}$$

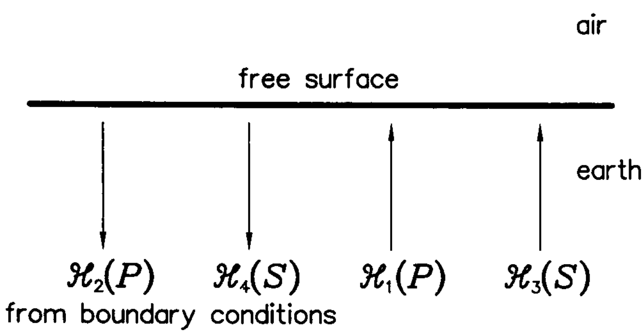

FIG. 1. The diagram displays the four propagating modes perpendicular to the interface. The incoming characteristic variables $\mathcal{H}_2$ and $\mathcal{H}_4$ are calculated from the boundary conditions.

$$\dot{\sigma}_{zz} = 0, \tag{19d}$$

$$\dot{\sigma}_{xz} = 0, \tag{19e}$$

$$\ddot{e}_{1\ell} = \phi_{1\ell}\left\{\frac{2\hat{\mu}}{\hat{\lambda}+2\hat{\mu}}\frac{\partial v_x}{\partial x} - \frac{1}{\hat{\lambda}+2\hat{\mu}}\right.$$

$$\left.\times\left[(\lambda+\mu)\sum_{\ell=1}^{L_1}\dot{e}_{1\ell} - \mu\sum_{\ell=1}^{L_2}\dot{e}_{2\ell}\right]\right\} - \frac{\dot{e}_{1\ell}}{\tau_{\sigma\ell}^{(1)}},$$

$$\ell = 1, \ldots, L_1, \tag{19f}$$

$$\ddot{e}_{2\ell} = \phi_{2\ell}\left\{\frac{2(\hat{\lambda}+\hat{\mu})}{\hat{\lambda}+2\hat{\mu}}\frac{\partial v_x}{\partial x} + \frac{1}{\hat{\lambda}+2\hat{\mu}}\left[(\lambda+\mu)\sum_{\ell=1}^{L_1}\dot{e}_{1\ell}\right.\right.$$

$$\left.\left.- \mu\sum_{\ell=1}^{L_2}\dot{e}_{2\ell}\right]\right\} - \frac{\dot{e}_{2\ell}}{\tau_{\sigma\ell}^{(2)}},$$

$$\ell = 1, \ldots, L_2, \tag{19g}$$

$$\ddot{e}_{3\ell} = -\phi_{2\ell}\frac{\mu}{\hat{\mu}}\sum_{\ell=1}^{L_2}\dot{e}_{3\ell} - \frac{\dot{e}_{3\ell}}{\tau_{\sigma\ell}^{(2)}}, \qquad \ell = 1, \ldots, L_2. \tag{19h}$$

These are the equations to be used at the free surface. Denoting the variables given in equations (1), (2), and (5) with the superscript (*old*), and the variables given in equations (19) with the superscript (*new*), the latter read

$$\dot{v}_x^{(new)} = \dot{v}_x^{(old)} + \frac{1}{\rho c_S}\dot{\sigma}_{xz}^{(old)}, \tag{20a}$$

$$\dot{v}_z^{(new)} = \dot{v}_z^{(old)} + \frac{1}{\rho c_P}\dot{\sigma}_{zz}^{(old)}, \tag{20b}$$

$$\dot{\sigma}_{xx}^{(new)} = \dot{\sigma}_{xx}^{(old)} - \frac{\hat{\lambda}}{(\hat{\lambda}+2\hat{\mu})}\dot{\sigma}_{zz}^{(old)}, \tag{20c}$$

$$\dot{\sigma}_{zz}^{(new)} = 0, \tag{20d}$$

$$\dot{\sigma}_{xz}^{(new)} = 0, \tag{20e}$$

$$\ddot{e}_{1\ell}^{(new)} = \ddot{e}_{1\ell}^{(old)} - \frac{\phi_{1\ell}}{\hat{\lambda}+2\hat{\mu}}\dot{\sigma}_{zz}^{(old)}, \qquad \ell = 1, \ldots, L_1, \tag{20f}$$

$$\ddot{e}_{2\ell}^{(new)} = \ddot{e}_{2\ell}^{(old)} + \frac{\phi_{2\ell}}{\hat{\lambda}+2\hat{\mu}}\dot{\sigma}_{zz}^{(old)}, \qquad \ell = 1, \ldots, L_2, \tag{20g}$$

$$\ddot{e}_{3\ell}^{(new)} = \ddot{e}_{3\ell}^{(old)} - \frac{\phi_{2\ell}}{\hat{\mu}}\dot{\sigma}_{xz}^{(old)}, \qquad \ell = 1, \ldots, L_2. \tag{20h}$$

This notation is consistent with that used in Bayliss et al., (1986), and Kosloff et al., (1990).

THE MODELING SCHEME

A seismic reflection survey involves an explosion close to the surface and the recording of the earth response at receivers located at the surface. The solution is discretized in time as well as in space. This modeling algorithm consists in the calculation of the spatial derivatives, incorporation of the boundary conditions, and time integration. Pseudospectral methods are used to compute the spatial derivatives. In the horizontal direction, the Fourier pseudospectral method is used since it is efficient in terms of the number of grid points per wavelength. Then, in the horizontal direction the coordinates of the sampling points are given by

$$x_i = \frac{x_{\max}}{N_X}(i-1), \; i = 1, \ldots, N_X, \tag{21}$$

where $x_{\max}$ is the maximum distance and N_X is the number of grid points. For a given function $f(x)$, with transform $\tilde{f}$, derivatives are computed as

$$\frac{d\tilde{f}}{dx} = ik_x\tilde{f},$$

$$k_x = \frac{2\pi}{N_X D_X}j,$$

$$j = -\frac{N_X-1}{2}, \ldots, \frac{N_X+1}{2} \tag{22}$$

for odd N_X, where k_x is the discrete wavenumber and D_X is the grid size. However, the Fourier method is not appropriate for the vertical direction since it cannot handle the recording configuration mentioned before, with source and receivers close to the free surface (Kosloff et al., 1990). Thus, in the vertical direction, the modified Chebychev pseudospectral method is used. The method is nonperiodic and provides high accuracy and resolution at the surface. When solving the problem with an explicit time marching algorithm, the conventional Chebychev differential operator requires time steps of the order $O(N^{-2})$, where N is the number of grid points. A new algorithm, based on a coordinate transformation, allows time steps of order $O(N^{-1})$, which are those also required by the Fourier method.

The N_Z sampling points are defined by

$$z_i = g(\zeta_i), \qquad \zeta_i = \cos\left(\frac{\pi i}{N_Z}\right), \qquad i = 0, \ldots, N_Z - 1, \tag{23}$$

where ζ_i are the Gauss-Lobato collocation points, and $g(\zeta)$ is a grid stretching function that stretches the super fine Chebychev grid near the free surface to have a minimum grid size $D_Z = O(N_Z^{-1})$, thus requiring a less severe stability condition. Figures 2a and b represent the conventional and modified Chebychev grids, respectively. In particular, the density of grid points at the lower boundary has been reduced considerably since a fine grid is not necessary there. The vertical derivatives are calculated by the chain rule,

$$\frac{df}{dz} = \frac{df}{d\zeta}\frac{d\zeta}{dz}, \tag{24}$$

The derivative with respect to ζ at the ith sampling point is

$$\frac{df}{d\zeta}(\zeta_i) = \sum_{k=1}^{N_Z - 1} b_k Q_k(\zeta_i), \quad i = 0, \ldots, N_Z - 1, \tag{25}$$

where Q_k are Chebychev polynomials, and b_k are the coefficients for the derivatives (Gottlieb and Orszag, 1977). Integration of the viscoelastic wave equation in unbounded media is carried out with spectral accuracy by using the algorithm given in Tal-Ezer et al., (1990). This technique is adapted to the Fourier pseudospectral method, which is used to compute the spatial derivatives in both the vertical and horizontal directions. Unfortunately, the algorithm is not efficient when Chebychev differential operators are used since the eigenvalues of the collocation matrix are not near the imaginary axis of the complex wavenumber plane, unlike with the Fourier differential operator.

An efficient time integration algorithm is the fourth-order Runge-Kutta method (e.g., Canuto et al., 1988). Let the spatial derivative operation in equation (8) be abbreviated to

$$\underset{\sim}{\mathbf{M}} = \underset{\sim}{\mathbf{A}} \frac{\partial}{\partial x} + \underset{\sim}{\mathbf{B}} \frac{\partial}{\partial z}. \tag{26}$$

If dt is the time step, the solution at time $(n+1)\,dt$, $\mathbf{V}^{n+1}$, is obtained in terms of the solution at time ndt, $\mathbf{V}^n$, as

$$\mathbf{V}^{n+1} = \mathbf{V}^n + \frac{1}{6} dt\,(\Delta_1 + 2\Delta_2 + 2\Delta_3 + \Delta_4), \tag{27a}$$

where

$$\Delta_1 = \underset{\sim}{\mathbf{M}}\mathbf{V}^n + \mathbf{D}^n, \tag{27b}$$

$$\Delta_2 = \underset{\sim}{\mathbf{M}}\left(\mathbf{V}^n + \frac{dt}{2}\Delta_1\right) + \mathbf{D}^{n+1/2}, \tag{27c}$$

$$\Delta_3 = \underset{\sim}{\mathbf{M}}\left(\mathbf{V}^n + \frac{dt}{2}\Delta_2\right) + \mathbf{D}^{n+1/2}, \tag{27d}$$

$$\Delta_4 = \underset{\sim}{\mathbf{M}}(\mathbf{V}^n + dt\Delta_3) + \mathbf{D}^{n+1}. \tag{27e}$$

As mentioned before, a favorable stability condition is achieved with $dt = O(N^{-1})$.

At the free surface, the boundary conditions are applied by solving equations (19), whereas for the bottom boundary, nonreflecting conditions are implemented. The appropriate equations for this case are given in the Appendix. Since for nonvertical incidence, the incoming waves may not be eliminated completely, an absorbing strip can be added to improve the efficiency (Kosloff and Kosloff, 1986). Similar absorbing regions can be placed along the boundaries in the horizontal direction to avoid wraparound caused by the periodic properties of the Fourier method. The mesh configuration is displayed in Figure 3. The boundary conditions are automatically implemented when solving equations (20) with the appropriate operator $\underset{\sim}{\mathbf{M}}$ obtained from equations (19) for the free surface, and equations (A-3) for the nonreflecting boundary at the bottom of the model.

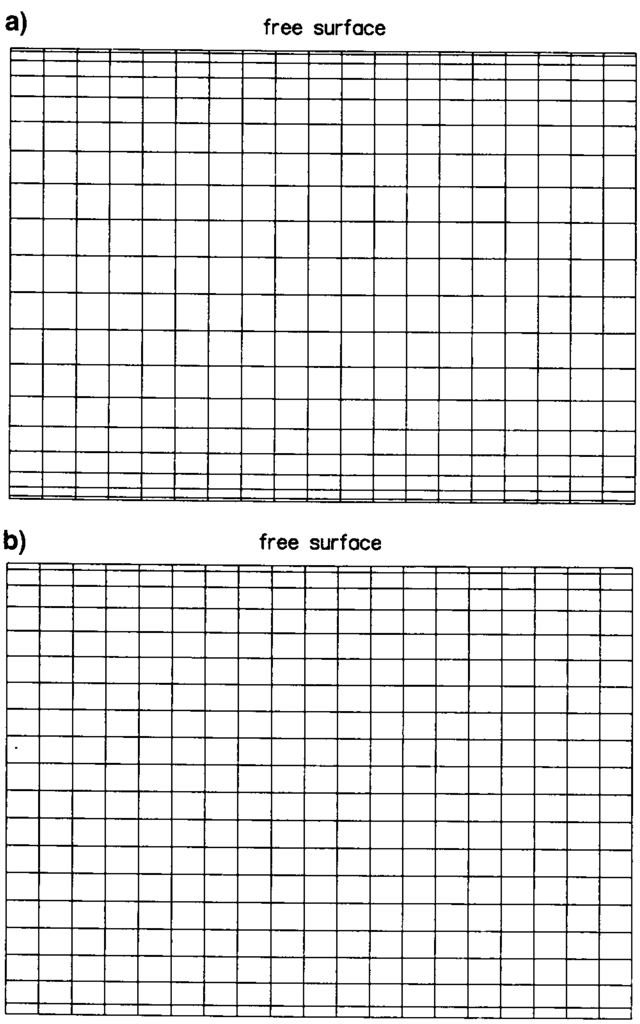

FIG. 2. (a) Chebychev and (b) modified Chebychev grids in the vertical direction. The stretching overcomes the severe stability condition imposed by the conventional Chebychev grid due to the very fine sampling at the boundaries. The horizontal sampling points are equidistant since the Fourier method is used to compute the horizontal derivatives.

EXAMPLES

The following numerical experiments test the modeling scheme. Since there is no analytical solution for anelastic surface waves, the aim is to verify whether the anelastic effects and different events come out correctly in the presence of free surface boundary conditions. The first example represents an unconsolidated weathering zone, while the second example introduces an elastic-anelastic vertical interface.

HOMOGENEOUS WEATHERING ZONE

The most simple structure is a homogeneous viscoelastic half-space bounded by a free surface. The low-frequency limit compressional and shear-wave velocities are taken as V_P = 2000 m/s and V_S = 1155 m/s, respectively, corresponding to a Poisson solid; the density is $\rho = 1$ kg/m^3. Two sets of relaxation times, indicated in Table 1, are used ($L_1 = L_2 = 2$), such that the quality factors are nearly constant over the exploration seismic band. The quality factors for P waves, S waves, and bulk waves turn out to be Q_P = 30, Q_S = 20, and Q_k = 40, respectively. The structure may represent an unconsolidated weathering zone.

The calculations use a grid size of $N_X = 135$ and $N_Z = 81$, with uniform grid spacing $DX = 20$ m in the horizontal direction, and a largest vertical grid spacing of $DZ = 20$ m. To prevent wavefield wraparound in the horizontal direction, an absorbing region of 18 points surrounds the numerical mesh. A vertical point force is applied at grid point 20 at a depth of 1.8 m. The source is a shifted zero-phase Ricker wavelet with a central frequency of 11 Hz, and a high cutoff frequency of 22 Hz. At the dominant frequency, the P and S phase velocities are 2052 m/s and 1200 m/s, respectively. These values indicate that significant dispersion is expected, with the anelastic wavefields faster than the low-frequency elastic wavefields. The numerical solution is propagated to 2 s with a time step of 1 ms.

A Poisson solid has $\lambda = \mu$, so that $V_P = \sqrt{3}\, V_S$. The equation for the Rayleigh wave complex velocity $V(\omega)$ in a Poisson solid is given by (Carcione, 1992):

$$3q^3 - 24q^2 + 56q - 32 = 0, \qquad q = \frac{V^2}{\bar{V}_S^2}, \tag{28}$$

where (Carcione et al., 1988),

$$\bar{V}_S = V_S \sqrt{\sum_{\ell=1}^{L_2} \frac{1 + i\tau_{\epsilon\ell}^{(2)}}{1 + i\tau_{\sigma\ell}^{(2)}}}, \tag{29}$$

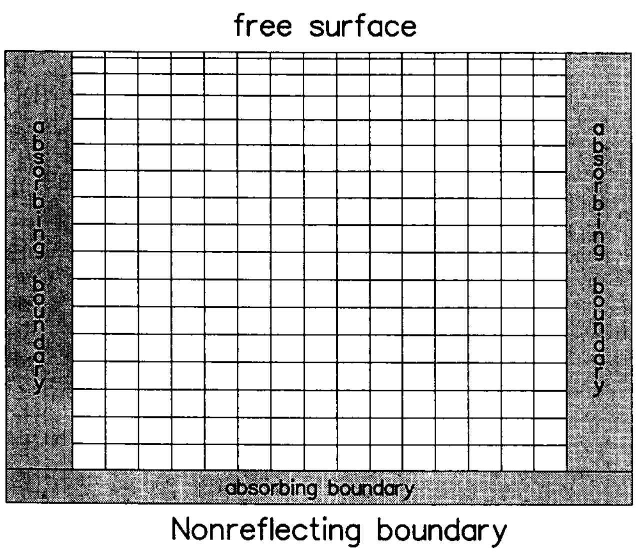

FIG. 3. Numerical mesh and imposed boundary conditions. At the bottom of the grid the incoming waves are eliminated by the boundary treatment.

Table 1. Relaxation times.

ℓ	$\tau_{\epsilon\ell}^{(1)}$ (s)	$\tau_{\sigma\ell}^{(1)}$ (s)	$\tau_{\epsilon\ell}^{(2)}$ (s)	$\tau_{\sigma\ell}^{(2)}$ (s)
1	0.0332577	0.0304655	0.0352443	0.0287482
2	0.0033257	0.0030465	0.0029370	0.0023957
1	0.0325305	0.0311465	0.0332577	0.0304655
2	0.0032530	0.0031146	0.0033257	0.0030465

is the complex velocity of shear waves.

Equation (28) has three real roots, but only one has a physical meaning: $q = 2 - 2/\sqrt{3}$, which corresponds to the anelastic Rayleigh wave. It is proved in Carcione (1992) that the quality factors per unit volume at the surface and per unit area are the same, and equal to the S-wave quality factor:

$$Q = \frac{\mathrm{Re}\,[\bar{V}_S^2]}{\mathrm{Im}\,[\bar{V}_S^2]}. \tag{30}$$

Moreover, the velocity of the energy equals the phase velocity which is given by

$$c = \mathrm{Re}^{-1}\left[\frac{1}{V}\right]. \tag{31}$$

Thus, the phase velocity at the central frequency of the source (11 Hz) is $c = 1104$ m/s.

Figure 4 compares elastic and anelastic snapshots, where (a) $t = 0.75$ s, and (b) $t = 1.25$ s. The different events are indicated in the elastic horizontal component. The shear head wave connects the P and S waves, and makes an angle of $\theta = \sin^{-1} V_S/V_P \simeq 35$ with the free surface. The Rayleigh wave is confined to the surface, which is a node (zero amplitude) for the S wave since the source is a vertical impulse. At $t = 1.25$ s, the surface wave has attenuated considerably and precedes the elastic Rayleigh wave by a distance of approximately 50 m. The latter travels with a velocity of $c_e = 0.9194\ V_S = 1062$ m/s, which compared to 1104 m/s gives nearly 50 m in 1.25 s traveltime.

The seismic response is recorded at the same depth as the source position. Figure 5 compares elastic and anelastic seismograms, (a) horizontal components, and (b) vertical components. As can be appreciated in the elastic horizontal component, the compressional wave loses amplitude with time due to geometrical spreading, while the Rayleigh wave keeps the same amplitude since it is confined to the surface. The situation changes in the anelastic medium where the attenuation and velocity dispersion have considerable affect on the surface wave.

WEATHERING ZONE WITH A VERTICAL INTERFACE

This model consists of a vertical interface separating an elastic medium from an anelastic region bounded at the top by a free surface. The structure, together with the material parameters, is represented in Figure 6, where the relaxed or low-frequency limit wave velocities are indicated. The numerical grid, source type, and central frequency are those of the first example. The experiment tests the modeling algorithm when the material parameters vary laterally, particularly in the case of a strong contrast in the anelastic properties.

Compared to the previous example, the structure is more complex and more events take place, as can be appreciated in Figure 7, where snapshots for (a) $t = 0.75$ s, and (b) $t = 1.25$ s are displayed; R denotes the Rayleigh wave. In Figure 7a, only the P wavefront and the head wave have reached the interface, while in Figure 7b, the Rayleigh wave has been transmitted and reflected and has created a Stoneley wave traveling downward along the interface. Clearly, anelasticity causes strong attenuation and velocity dispersion; compare

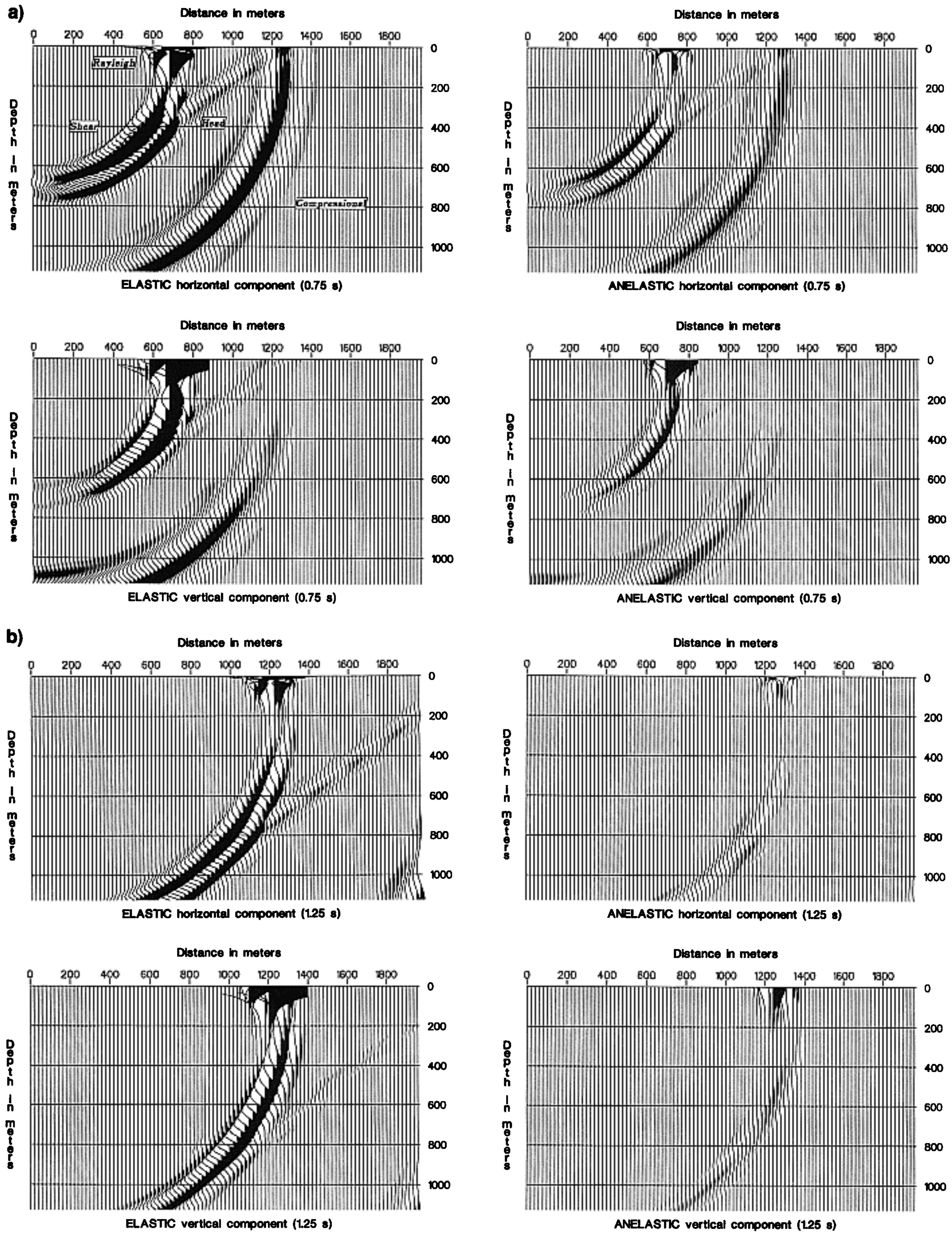

FIG. 4. Comparison between elastic and anelastic wavefields propagating in a homogeneous weathering zone, (a) $t = 0.75$ s and (b) $t = 1.25$ s. Relaxed P and S wave velocities are 2000 m/s and 1155 m/s, respectively, while quality factors for P waves, S waves, and bulk waves are $Q_P = 30$, $Q_S = 20$, and $Q_k = 40$, respectively. The source is a vertical point force of the Ricker type with a central frequency of 11 Hz located at a depth of 1.8 m.

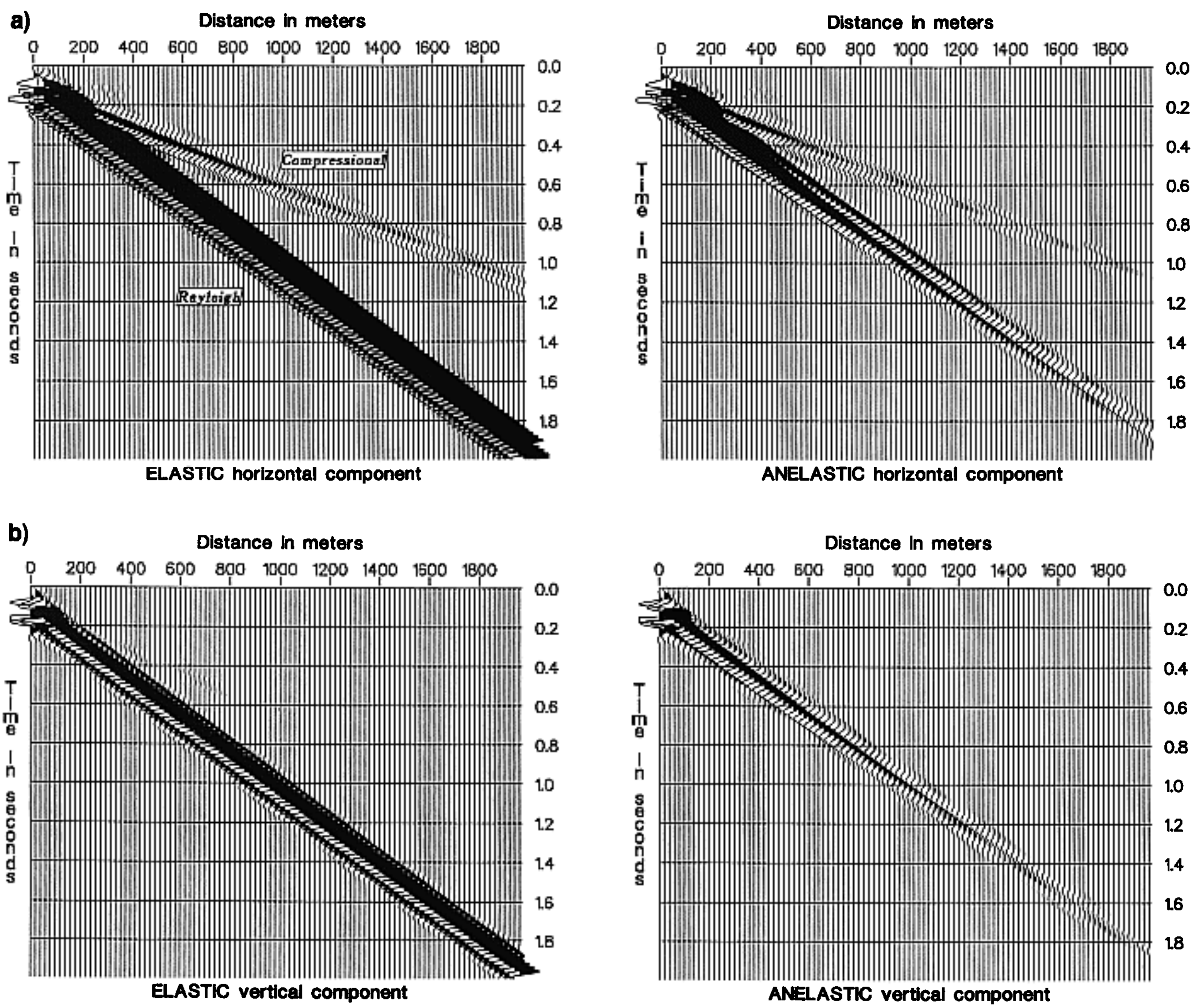

FIG. 5. Comparison between elastic and anelastic seismograms recorded at the surface of a homogeneous weathering zone: (a) horizontal components and (b) vertical components.

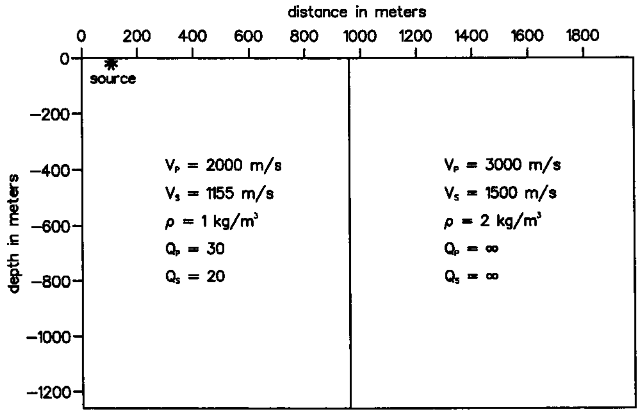

FIG. 6. Geological model of a weathering zone with a vertical interface. The medium on the left side is anelastic where the relaxed velocities are indicated. The medium on the right side is purely elastic. The source is the same as in Figure 4.

for instance, the position of the Stoneley wave in the elastic and anelastic snapshots.

A good test of the effectiveness of the boundary conditions is the analysis of the anelastic properties of the Rayleigh wave at both sides of the interface. This can be done in the synthetic seismograms represented in Figure 8, recorded at the same depth as the source along the free surface. The different events are identified in the elastic horizontal component. Also indicated in the Figure are converted body waves originating from the collision of the Rayleigh wave with the interface. It is clear how the surface wave is dissipated in the left side of the interface (up to approximately 1 s traveltime) and keeps its amplitude after crossing the interface since the medium there is elastic. On the other hand, the reflected Rayleigh wave attenuates almost completely after 2 s propagating time.

CONCLUSIONS

The present forward modeling scheme simulates anelastic surface waves with spectral accuracy in the calculations of the spatial derivatives. The examples show that the modeling correctly reproduces the anelastic properties even in the presence of strong contrasts in the material parameters, especially the quality factors. Further research is required to determine if a spectral time integration technique can be used with this technique. The modeling will be very useful for analyzing the

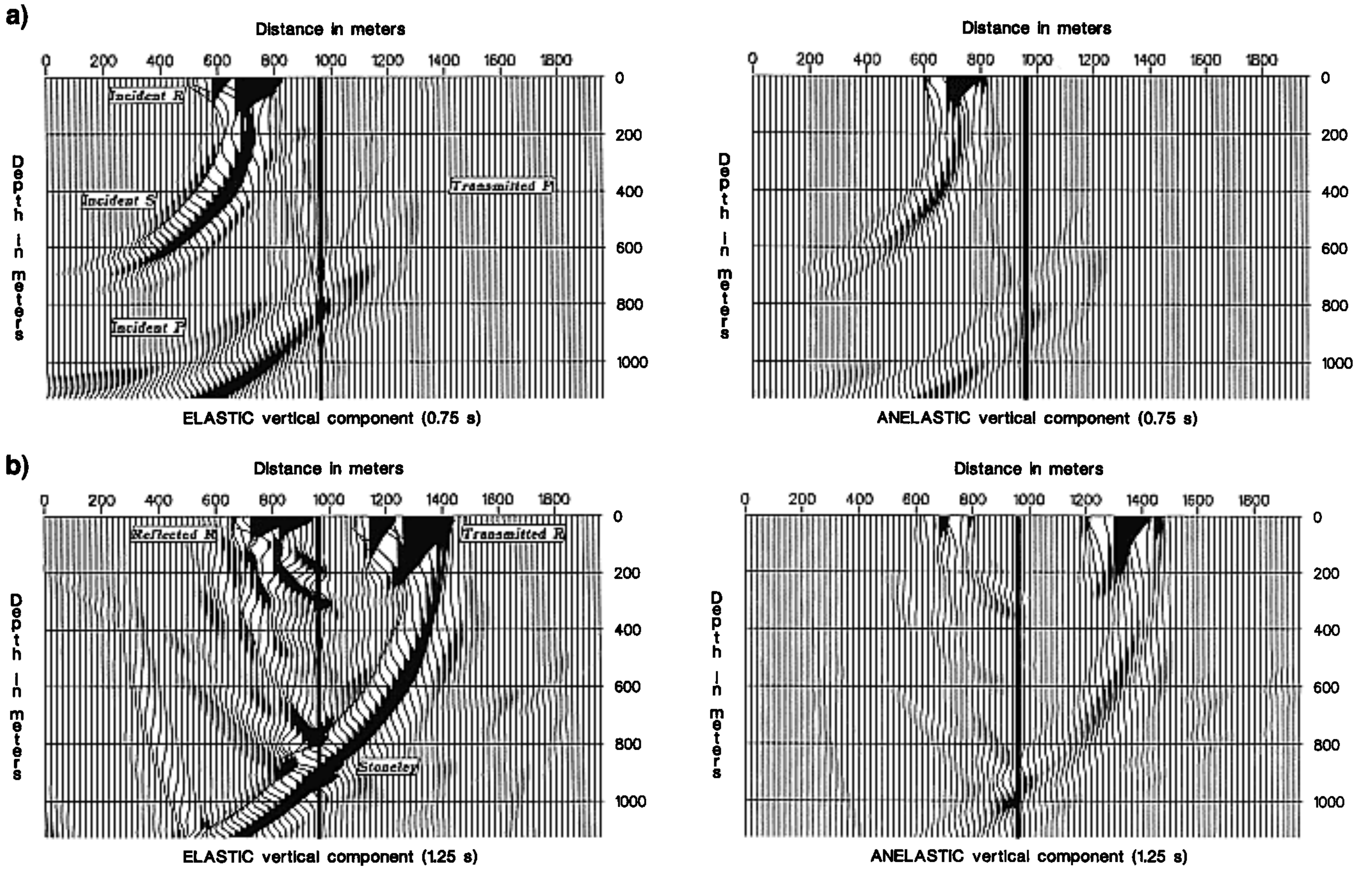

FIG. 7. Comparison between elastic and anelastic wavefields propagating in a weathering zone with a vertical interface: (a) t = 0.75 s and (b) t = 1.25 s. R indicates the Rayleigh wave.

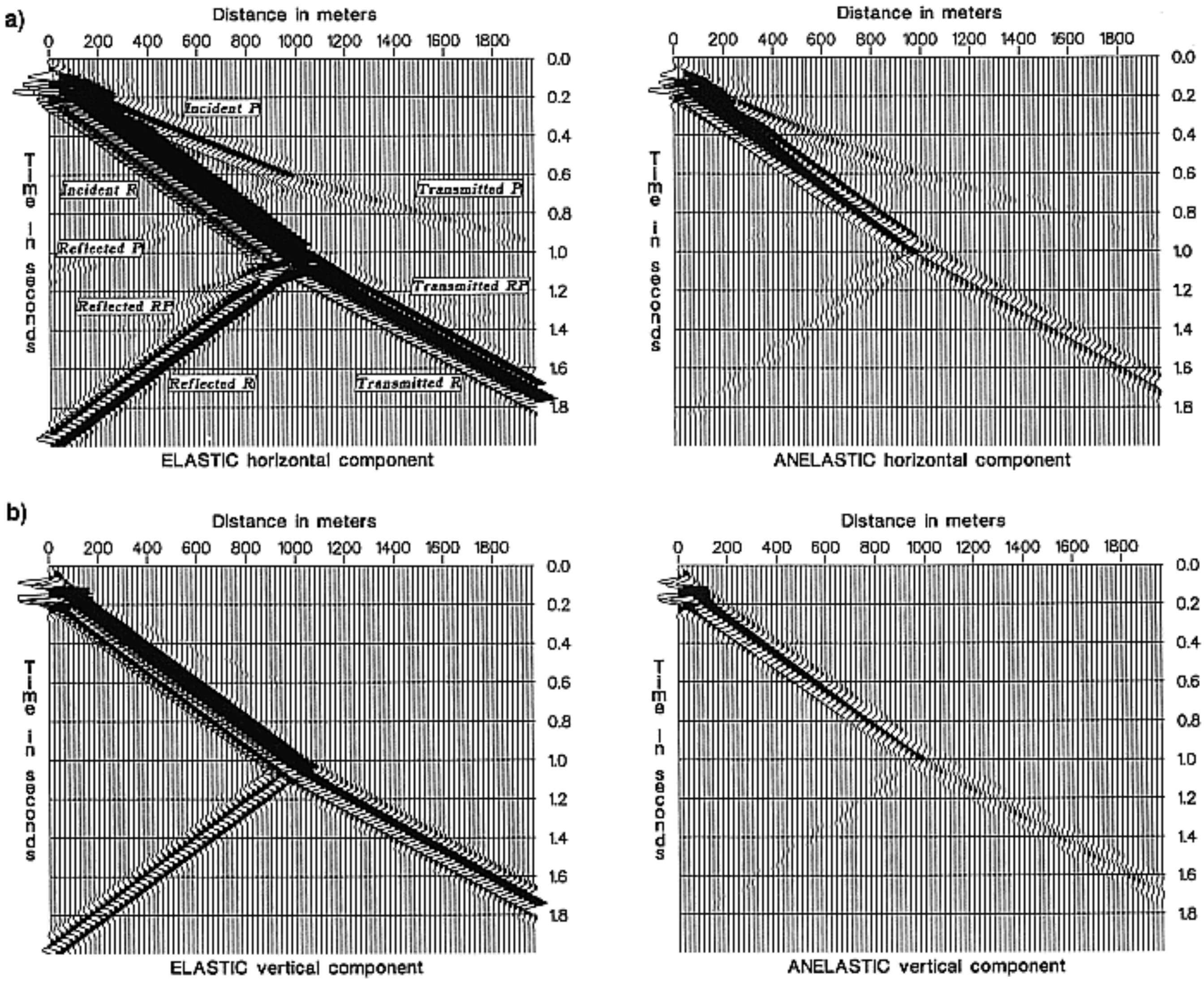

FIG. 8. Comparison between elastic and anelastic seismograms recorded at the surface of a weathering zone with a vertical interface: (a) horizontal components and (b) vertical components. *R* indicates the Rayleigh wave.

physical properties of Rayleigh waves and the existence of a new surface wave in anelastic media. Extension to 3-D and the anisotropic-viscoelastic rheology introduced in Carcione (1990) will also be investigated in future work.

ACKNOWLEDGMENTS

This work was supported in part by the Commission of the European Communities under the GEOSCIENCE project.

REFERENCES

Bayliss, A., Jordan, K. E., LeMesurier, B. J., and Turkel, E., 1986. A fourth-order accurate finite-difference scheme for the computation of elastic waves: Bull. Seis. Soc. Am., **76**, 1115–1132.

Canuto, C., Hussaini, M. Y., Quarteroni, A., and Zang, T. A., 1988, Spectral methods in fluid dynamics: Springer-Verlag New York, Inc. 450.

Carcione, J. M., 1990, Wave propagation in anisotropic linear viscoelastic media: Theory and simulated wavefields: Geophys. Int., **101**, 739–750.

——— 1992, Rayleigh waves in isotropic-viscoelastic media: Geophys. J. Int., **108**, 453–464.

Carcione, J. M., and Behle, A., 1989, Two-dimensional and three-dimensional forward modeling in isotropic-viscoelastic media: 59th Ann. Internat. Mtg., Soc. Expl. Geophys., Expanded Abstracts, 1050–1053.

Carcione, J. M., Kosloff, D., and Kosloff, R., 1988, Wave propagation simulation in a linear viscoelastic medium: Geophys. J. Roy. Astr. Soc., **95**, 597–611.

Gottlieb, D., and Orszag, S. A., 1977, Numerical analysis of spectral methods: Theory and applications: CBMS Reg. Conf. Series in Appl. Math. 26, Soc. Ind. and Appl. Math.

Kosloff, D., Kessler, D., Queiroz Filho, A., Tessmer, E., Behle, A., and Strahilevitz, R., 1990, Solution of the equations of dynamic elasticity by a Chebychev spectral method: Geophysics, **55**, 734–748.

Kosloff, R., and Kosloff, D., 1986, Absorbing boundaries for wave propagation problems: J. Comp. Phys., **63**, 363–376.

Tal-Ezer, H., Carcione, J. M., and Kosloff, D., 1990, An accurate and efficient scheme for wave propagation in a linear viscoelastic medium: Geophysics, **55**, 1366–1379.

Thomson, K. W., 1990, Time-dependent boundary conditions for hyperbolic systems, II: J. Comp. Phys., **89**, 439–461.

APPENDIX

NONREFLECTING BOUNDARY CONDITIONS

Suppose that $z = a = -z_0$ is a boundary of the numerical mesh. Since this is not a physical boundary, the incoming wave must be suppressed to avoid nonphysical reflections.

The incoming variables are $\mathcal{H}_1$ and $\mathcal{H}_3$. The first and third components of equation (12) give the following characteristics equations:

$$-\frac{\partial}{\partial t}\left[\frac{1}{\sqrt{2}}\left(v_z + \frac{1}{\rho c_P}\sigma_{zz}\right)\right] + \mathcal{H}_1 + \frac{1}{\sqrt{2}}\left\{\frac{1}{\rho}\frac{\partial \sigma_{xz}}{\partial x} + \frac{1}{\rho c_P}\left[\hat{\lambda}\frac{\partial v_x}{\partial x} + (\lambda + \mu)\sum_{\ell=1}^{L_1} \dot{e}_{1\ell} - \mu \sum_{\ell=1}^{L_2} \dot{e}_{2\ell}\right] + f_z\right\} = 0, \tag{A-1a}$$

$$-\frac{\partial}{\partial t}\left[\frac{1}{\sqrt{2}}\left(v_x + \frac{1}{\rho c_S}\sigma_{xz}\right)\right] + \mathcal{H}_3 + \frac{1}{\sqrt{2}} \times \left[\frac{1}{\rho}\frac{\partial \sigma_{xx}}{\partial x} + \frac{1}{\rho c_S}\left(\hat{\mu}\frac{\partial v_z}{\partial x} + \mu \sum_{\ell=1}^{L_2} \dot{e}_{3\ell}\right) + f_x\right] = 0. \tag{A-1b}$$

These equations contain the time derivatives of the amplitudes of the incoming characteristic waves. Imposing constant amplitudes in time is equivalent to suppressing the incoming waves. This can be done by choosing

$$\mathcal{H}_1 = -\frac{1}{\sqrt{2}}\left\{\frac{1}{\rho}\frac{\partial \sigma_{xz}}{\partial x} + \frac{1}{\rho c_P}\left[\hat{\lambda}\frac{\partial v_x}{\partial x} + (\lambda + \mu) \times \sum_{\ell=1}^{L_1} \dot{e}_{1\ell} - \mu \sum_{\ell=1}^{L_2} \dot{e}_{2\ell}\right] + f_z\right\}, \tag{A-2a}$$

$$\mathcal{H}_3 = -\frac{1}{\sqrt{2}}\left[\frac{1}{\rho}\frac{\partial \sigma_{xx}}{\partial x} + \frac{1}{\rho c_S}\left(\hat{\mu}\frac{\partial v_z}{\partial x} + \mu \sum_{\ell=1}^{L_2} \dot{e}_{3\ell}\right) + f_x\right], \tag{A-2b}$$

while $\mathcal{H}_2$ and $\mathcal{H}_4$ are computed from equations (16b) and (16d), respectively. Then, substituting $\mathcal{H}$ into equations (12) gives at the nonreflecting boundary:

$$\dot{v}_x^{(new)} = \frac{1}{2}\left(\dot{v}_x^{(old)} - \frac{1}{\rho c_S}\dot{\sigma}_{xz}^{(old)}\right), \tag{A-3a}$$

$$\dot{v}_z^{(new)} = \frac{1}{2}\left(\dot{v}_z^{(old)} - \frac{1}{\rho c_P}\dot{\sigma}_{zz}^{(old)}\right), \tag{A-3b}$$

$$\dot{\sigma}_{xx}^{(new)} = \dot{\sigma}_{xx}^{(old)} - \frac{\hat{\lambda}}{2(\hat{\lambda} + 2\hat{\mu})}(\dot{\sigma}_{zz}^{(old)} + \rho c_P \dot{v}_z^{(old)}), \tag{A-3c}$$

$$\dot{\sigma}_{zz}^{(new)} = \frac{1}{2}(\dot{\sigma}_{zz}^{(old)} - \rho c_P \dot{v}_z^{(old)}), \tag{A-3d}$$

$$\dot{\sigma}_{xz}^{(new)} = \frac{1}{2}(\dot{\sigma}_{xz}^{(old)} - \rho c_S \dot{v}_x^{(old)}), \tag{A-3e}$$

$$\ddot{e}_{1\ell}^{(new)} = \ddot{e}_{1\ell}^{(old)} - \frac{\phi_{1\ell}}{2(\hat{\lambda} + 2\hat{\mu})}(\dot{\sigma}_{zz}^{(old)} + \rho c_P \dot{v}_z^{(old)}), \quad \ell = 1, \ldots, L_1, \tag{A-3f}$$

$$\ddot{e}_{2\ell}^{(new)} = \ddot{e}_{2\ell}^{(old)} + \frac{\phi_{2\ell}}{2(\hat{\lambda} + 2\hat{\mu})}(\dot{\sigma}_{zz}^{(old)} + \rho c_P \dot{v}_z^{(old)}), \quad \ell = 1, \ldots, L_2, \tag{A-3g}$$

$$\ddot{e}_{3\ell}^{(new)} = \ddot{e}_{3\ell}^{(old)} - \frac{\phi_{2\ell}}{2\hat{\mu}}(\dot{\sigma}_{xz}^{(old)} + \rho c_S \dot{v}_x^{(old)}), \quad \ell = 1, \ldots, L_2. \tag{A-3h}$$